

# Optical Engineering

OpticalEngineering.SPIEDigitalLibrary.org

## **Thermal loading effects on Nd:YAG solar-laser performance in end-pumping and side-pumping configurations: a review**

Said Mehellou  
Ferhat Rehouma  
Noureddine Hamrouni  
Leila Bouras

**SPIE.**

Said Mehellou, Ferhat Rehouma, Noureddine Hamrouni, Leila Bouras, "Thermal loading effects on Nd:YAG solar-laser performance in end-pumping and side-pumping configurations: a review," *Opt. Eng.* **57**(12), 120902 (2018), doi: 10.1117/1.OE.57.12.120902.

# Thermal loading effects on Nd:YAG solar-laser performance in end-pumping and side-pumping configurations: a review

Said Mehellou,<sup>a,b,\*</sup> Ferhat Rehouma,<sup>a,b</sup> Nouredine Hamrouni,<sup>a,b</sup> and Leila Bouras<sup>a,b</sup>

<sup>a</sup>EHL University, Laboratory of Exploitation and Valorization of Saharian Energy Resources (LEVRES), Eloued, Algeria

<sup>b</sup>Echahid Hamma Lakhdar University, Eloued, Algeria

**Abstract.** Solar-pumped solid-state lasers are promising for many applications. Among the potential applications of solar lasers are Earth, ocean, and atmospheric sensing; laser beaming; deep space communications; and energy support in space. A solar laser has also a large potential for many terrestrial applications, e.g., high temperature materials processing, magnesium–hydrogen energy cycle and so on. Solar-pumped lasers are natural candidates for applications where sunlight is plentiful and other forms of energy sources are scarce. As solar energy is the main continuous energy source in space, this technology becomes particularly attractive for space-based applications. Compared with electrically powered lasers, solar-pumped lasers benefit from simplicity and reliability because of the complete elimination of the electrical power generation and conditioning equipment. Since the report of the first sun-pumped solid-state laser, several pumping schemes have been proposed for enhancing solar-laser performance. Although the most efficient solar-laser systems have end-pumping approaches, the thermal loading effects caused by nonuniform distribution of absorbed pump light in these pumping configurations negatively affect their efficiencies. The side-pumping configuration can present higher laser beam quality as it allows uniform absorption distribution along the laser rod axis and spreads the absorbed power within the laser medium, reducing the associated thermal loading problems. Here, we report a review of research carried out on Nd:YAG solar-lasers with continuous wave emission, using either end-pumping or side-pumping techniques with a special focus on the thermal loading effects on the solar-lasers performance. In the end-pumping configuration, record-high multimode collection efficiency of 32.1 W/m<sup>2</sup> is attained by pumping a 6-mm diameter, 95-mm length, Nd:YAG/YAG rod with 1.03 m<sup>2</sup> area Fresnel lens. However, large beam quality factors of ( $M_x^2 = M_y^2 = 61$ ) have been associated with this approach, resulting in poor beam quality. In fundamental-mode operating, TEM<sub>00</sub>-mode, with this pumping technique, the highest collection efficiency is 7.9 W/m<sup>2</sup> by pumping a 4-mm diameter, 35-mm length, Nd:YAG rod with 1.18-m<sup>2</sup> area parabolic mirror with the lowest beam quality factors of 1.2. In the side-pumping configuration, the multimode collection efficiency was quite low; in contrast, the beam quality factors are much reduced. Low beam quality factors of ( $M_x^2 = 8.9$ ) and ( $M_y^2 = 9.6$ ) are obtained by pumping a 4-mm diameter, 30-mm length, Nd:YAG rod with 2.88-m<sup>2</sup> area parabolic mirror with only 9.6 W/m<sup>2</sup> multimode collection efficiency. The highest multi-mode collection efficiency achieved with this pumping method is 11.7 W/m<sup>2</sup> by pumping a 7-mm diameter, 30-mm length, Cr:Nd:YAG rod with 2.88-m<sup>2</sup> area parabolic mirror. In the TEM<sub>00</sub>-mode regime, using the side-pumping method, the maximum collection efficiency is 4.0 W/m<sup>2</sup> by pumping a 4-mm diameter, 25-mm length, Nd:YAG rod with 1.13-m<sup>2</sup> area parabolic mirror. Beam quality factors <1.05 are reached by pumping a thin and long Nd:YAG rod (3-mm diameter and 50-mm length), with 1.18-m<sup>2</sup> area parabolic mirror. More importantly, a TEM<sub>00</sub>-mode solar-laser with 1.7% laser power stability is produced, being significantly more stable than the previous TEM<sub>00</sub>-mode solar-lasers. © 2018 Society of Photo-Optical Instrumentation Engineers (SPIE) [DOI: [10.1117/1.OE.57.12.120902](https://doi.org/10.1117/1.OE.57.12.120902)]

Keywords: solar-pumped laser; end- and side-pumping configurations; TEM<sub>00</sub>-mode; thermal loading effect; collection efficiency; laser power stability.

Paper 181267V received Sep. 10, 2018; accepted for publication Nov. 27, 2018; published online Dec. 21, 2018.

## 1 Introduction

The idea of directly converting incoherent and broadband solar radiation into coherent and narrowband laser radiation has emerged shortly after the invention of laser.<sup>1</sup> Since the first report of “A sun-pumped continuous-wave one-watt laser” in 1966,<sup>1</sup> optical and laser material advances have continued to improve solar-laser performance.

By placing a Nd:YAG crystal directly into the focal region of a large primary parabolic concentrator, 18-W laser power was produced.<sup>2</sup> The introduction of the two-dimensional compound parabolic concentrator (2-D-CPC) and the

three-dimensional compound parabolic concentrator (3-D-CPC) further boosted the solar laser output power.<sup>3,4</sup> To enhance the spectral match between the emission spectrum of the pump radiation and the absorption spectrum of the laser medium, the crystals of different active materials were tested,<sup>5</sup> and others are codoped to improve their laser efficiency due to the enhanced absorption of sunlight spectrum, as the Cr-codoping to Nd:YAG, which will increase the possibility of efficient absorption and optical pumping rate to Nd ion in the solar spectrum.<sup>6,7</sup> Several pumping architectures have been proposed for solar-pumped solid-state lasers.<sup>8</sup> These lasers can have either side-pumping or end-pumping configurations. Although the most efficient laser systems have end-pumping approaches, the thermal loading effects caused by nonuniform distribution of pump light in these

\*Address all correspondence to Said Mehellou, E-mail: [saidmeh@gmail.com](mailto:saidmeh@gmail.com)

pumping configurations negatively affect their efficiencies. Side pumping is an effective configuration for power scaling and for producing high laser beam quality as it allows uniform absorption distribution along the laser rod axis and spreads the absorbed power within the laser medium, reducing the associated thermal loading problems.<sup>9</sup>

The development of solar lasers mainly concerns space power transmission and propulsion. New potential applications of solar lasers in space are emerging. These include Earth, ocean and atmospheric observation from space; detecting, illuminating and tracking hard targets in space; and deep space communications.

The use of solar pumped lasers on Earth seems constrained by economics. Therefore, prospective applications may be limited to those that require utilization of quantum effects and coherency of the laser to generate extremely high-value products and services when conventional and inexpensive means are ineffective or impossible. The main problem preventing wide spread use of solar-laser today is its low efficiency. Therefore, collection efficiency—defined by the ratio between laser output power and primary concentrator area<sup>10</sup>—is generally regarded as a primary figure of merit for solar-laser. The second is thermal problems worsening the efficiency as well as the beam quality. Lasers for many applications generally require high beam quality. This is not easy to achieve when the heat load of the laser crystal is high. The high heat load usually leads to very low efficiency, stability, and output power for fundamental-mode ( $TEM_{00}$ -mode) laser beams from solar-pumped lasers.<sup>11</sup>

For these purposes, we report here a review of research done on solar-laser field to show the thermal loading effects on Nd:YAG solar-lasers performance in end-pumping and side-pumping configurations. We discuss the thermal loading effects on the stability, the efficiency and the beam quality of solar-laser output-power and compare some of them with the previous experimental results, which give us a better explanation of the theoretical aspects.

## 2 Heat Generation in Solid-State Laser Materials

In solid-state lasers, a fraction of the absorbed pump energy converts to heat which acts as the heat source inside the laser

material.<sup>12,13</sup> As the heat load of the laser crystal is considered one of the main problems preventing wide spreading of solar-lasers, we address the issue of the heat generation in solid-state laser materials, both theoretically and experimentally.

### 2.1 Principle

The difference between the energy of pumping photons and the energy of laser's photons in optically pumped solid lasers is the main reason for the heat generated in the crystal lattice of the lasing medium in addition to heat resulting from transfer of nonlaser emitting upper levels—and the nonradiative relaxation from the pump band-to ground levels.<sup>14,15</sup> The absorption of pump radiation by the host material in turn causes the heating of the laser medium.<sup>15</sup>

Consequently, the heat generated inside the laser material acts as the heat source.<sup>12,13</sup> Spatial and time dependence of the heat source causes important effects on temperature distribution and warming rate of the laser medium, respectively. The spatial form is assumed to be the same shape as pumping light<sup>12,13</sup> and time dependence relates to the pumping procedure. Furthermore, depending on the laser medium configuration and cooling geometry, deposited heat may mostly flow through a preferable direction inside the laser medium and therefore causes thermal gradient. For instance, in traditional rod-shaped laser mediums with water cooling configuration, the main proportion of heat removal occurs through the radial direction which leads to the considerable radial thermal gradient inside the medium.

Figure 1 shows a schematic setup of pumping procedures for the rod-shaped laser medium. The dominant directions of heat removal which are associated with the laser medium configuration and cooling system geometry are illustrated.

The combination of the laser material heating by the absorbed pump-light and surface cooling required for heat extraction leads to a nonuniform temperature distribution in the laser rod resulting in a distortion of the laser beam. The degradation of the laser beam quality is due to thermal lensing.<sup>15</sup>

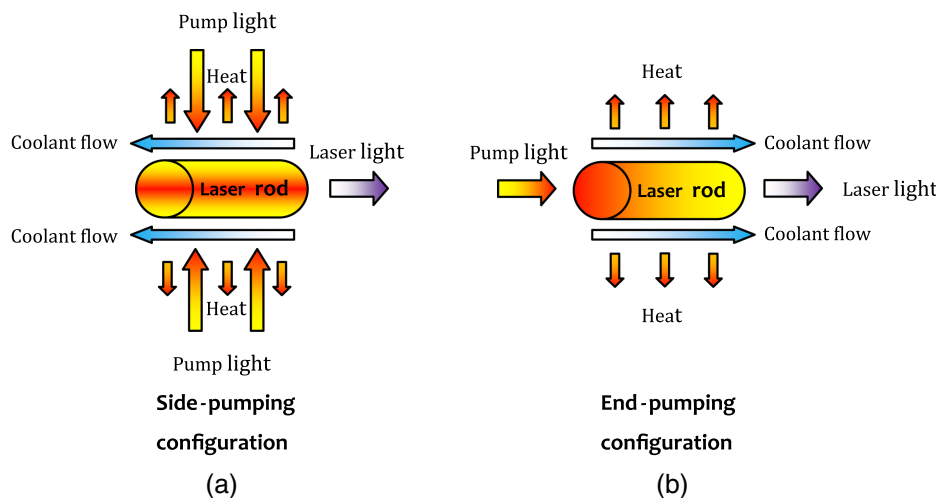


**Fig. 1** Schematic figure of preferable directions of heat removal in the rod-shaped laser medium in (a) side-pumping configuration and (b) end-pumping configuration.

## 2.2 Temperature Distribution

The particular temperature profile that exists in the laser material depends, to a large degree on the absorbed pump-light distribution resulting from the pumping methods, which can be either side-pumping or end-pumping techniques.

Using side-pumping configuration, uniform absorbed pump-light distribution can be achieved resulting in uniform heat generation within the laser medium. Although the end-pumping geometry leads to nonuniform absorbed pump-light distribution resulting in nonuniform heat generation into the laser medium.<sup>9</sup> Another way to decrease the thermal lensing effects than the generation of a uniform heat distribution inside the active medium is to use a lower dopant concentration and to act on the active medium geometry.

### 2.2.1 Side-pumping configuration

The pumping process is commonly performed by two methods, which are side-pumping and end-pumping laser techniques.

Figure 2 shows schematically a laser rod pumped by side-pumping technique. In this pumping method, the pump-light is transmitted uniformly to the laser rod by its cylindrical surface resulting in uniform absorbed pump-light distribution within the rod.

With the assumption of uniform internal heat generation achieved by the side-pumping configuration and the cooling along the cylindrical surface of a laser rod, the heat flow is strictly radial, and end effects and the small variation of coolant temperature in the axial direction can be neglected. The radial temperature distribution in a cylindrical rod with the thermal conductivity  $K_c$ , in which heat is uniformly generated at a rate  $Q$  per unit volume, is obtained from the 1-D heat conduction equation:<sup>15</sup>

$$\frac{d^2T}{dr^2} + \left(\frac{1}{r}\right)\left(\frac{dT}{dr}\right) + \frac{Q}{K_c} = 0 \quad (1)$$

The solution of this differential equation gives the steady-state temperature at any point along a radius of length  $r$ . With the boundary condition  $T(r_0)$  for  $r = r_0$ , where  $T(r_0)$  is the temperature at the rod surface and  $r_0$  is the radius of the rod, it follows that

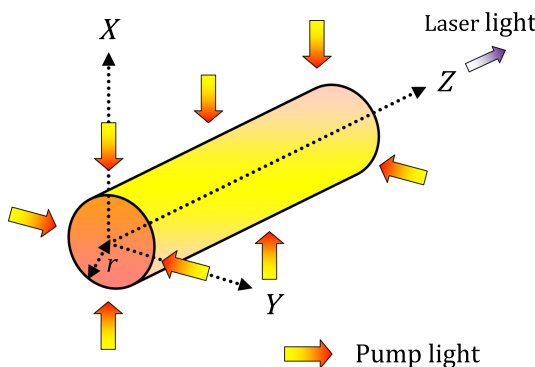


Fig. 2 Scheme of side-pumping method of a laser rod.

$$T(r) = T(r_0) + \left(\frac{Q}{4K}\right)(r_0^2 - r^2). \quad (2)$$

The temperature profile is parabolic, with the highest temperature at the center of the rod. The temperature gradients inside the rod are not a function of the surface temperature  $T(r_0)$  of the rod.

The thermal radial gradient as given by Eq. (2) introduces a radial variation of the refractive index. The change of the refractive index can be separated into a temperature and a stress dependent variation. Hence

$$n(r) = n_0 + \Delta(n)_T + \Delta(n)_\sigma, \quad (3)$$

where  $n(r)$  is the radial variation of the refractive index,  $n_0$  is the refractive index at the center of the rod,  $\Delta(n)_T$  and  $\Delta(n)_\sigma$  are the temperature and stress dependent changes of the refractive index, respectively.<sup>16</sup>

The thermal radial changes generated in the laser rod by using side-pumping method cause radial variations of the refractive index, which consequently lead to distortions of the laser beam. These distortions are due to temperature and stress-dependent variations of the refractive index.<sup>16</sup>

### 2.2.2 End-pumping configuration

In contrast to side-pumped laser systems, the heat deposition in end-pumped laser systems is very inhomogeneous. Figure 3 shows schematically a laser rod pumped by end-pumping technique. In this pumping method, the pump-light is transmitted to the laser rod through its end resulting in nonuniform absorbed pump-light distribution within the rod.

The very localized heat deposition resulting from the end-pumping method leads to highly nonuniform and complex temperature and stress profiles. In addition to the temperature and stress-dependent variations in the refractive index, the contribution of end bulging to the formation of a thermal lens can be substantial in end-pumped laser systems. Inhomogeneous local heating and nonuniform temperature distribution in the laser crystal lead to a degradation of the beam quality due to the highly aberrated nature of the thermal lens.<sup>15</sup>

An end-pumped laser rod has a temperature profile across the pumped region that follows the distribution of pump-light. From the edge of the pumped region, the temperature decays to the cooled cylindrical surface of the rod. Along the axis of the rod, the temperature profile will decay following the absorption profile of the pump-light, subject to the absorption law.

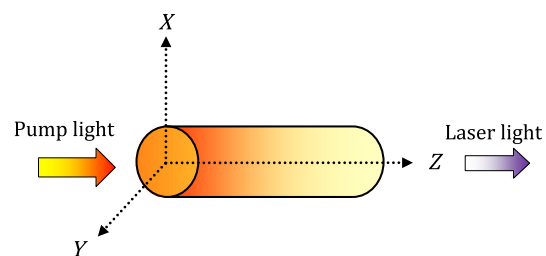


Fig. 3 Scheme of end-pumping method of a laser rod.

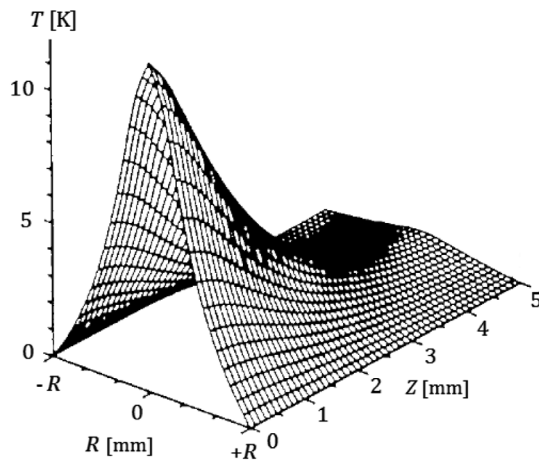


Fig. 4 Temperature distribution in an end-pumped laser rod.<sup>15</sup>

Figure 4 shows the calculated temperature distribution in a conductively cooled end-pumped laser rod.<sup>15</sup>

Assume homogeneous cooling on the surface of the laser rod, which means the temperature at each point along the axis of the rod is fixed and the thermal conductivity coefficient is independent of temperature.<sup>17</sup>

Under these assumptions, we can write a differential equation for thermal transfer in a cylindrical rod as follows:<sup>14,17–19</sup>

$$\frac{1}{r} \frac{\partial}{\partial r} \left[ r \frac{\partial T(r, z)}{\partial r} \right] + \frac{\partial^2 T(r, z)}{\partial z^2} = -\frac{Q(r, z)}{K_c}, \quad (4)$$

where  $T(r, z)$  is the temperature in Kelvin as a function of radial distance  $r$  and position along the  $z$ -axis,  $K_c$  is the thermal conductivity (W/m · K), and  $Q(r, z)$  is the heat in unit volume.

Thermal distribution within a laser crystal is a function of absorbed power density, which in turn takes the form of distributed light pumping at any vertical section on the axis of the laser crystal and parallel to the pumping beam. On the one hand, the intensity of light pumping decreases along the  $z$ -axis, subject to the law of absorption;  $(r, z)$  can be given in a number of forms depending on the beam shape.<sup>20</sup>

Boundary conditions are set based on the assumption that the side surface of the laser crystal is in direct contact with the coolant. The first boundary condition is the continuity of thermal flow through these surfaces<sup>17</sup> and the second boundary condition is  $T(r_s) = T_c$ , where  $T(r_s)$  is the temperature of the side surface of the laser crystal and  $T_c$  is the temperature of the coolant.

The change in the refractive index can be separated into two terms: the first part depends on the temperature distribution and the second part depends on the stress.<sup>14</sup> So, we can write

$$n(r, z) = n_0 + \Delta n(r, z)_T + \Delta n(r, z)_\epsilon, \quad (5)$$

where  $n(r, z)$  is the total index of refraction,  $\Delta n(r, z)_T$  is the part of index of refraction related to temperature,  $\Delta n(r, z)_\epsilon$  is the part of index of refraction related to stress, and  $n_0$  is the material index of refraction.

The very inhomogeneous heat deposition in end-pumped laser systems leads to significant thermal changes in the laser

rod, resulting in complex refractive index variations. The temperature and stress-dependent variations of the refractive index cause optical distortions that can severely degrade the optical quality of the laser beam and eventually limit the laser output power.<sup>15</sup>

Finally, it is very important to notice that the optical distortions due to the end-pumping method are substantial because of the complex refractive index variations, compared with those resulting from the side-pumping method, in which the significant variation of the refractive index is only radially.

### 3 Summary of Research Details for Exhibiting the Thermal Loads Effects on Nd:YAG Solar-Lasers Performance

The collection efficiency is generally regarded as a primary figure of merit for solar-lasers. The second is thermal problem worsening the efficiency as well as the beam quality.

The most important research in solar-laser field is summarized and discussed below in order to show, first that the end-pumping solar-laser systems are the most efficient; however, the thermal load effects caused by non-uniform distribution of pump light, typical in these pumping configurations, lead to a poor solar-laser beam quality. Second, that the side-pumping systems are the most effective for power scaling and for producing high solar-laser beam quality and stability as they give uniform absorption within the laser medium, reducing the associated thermal loading problems.

For clearly exhibiting the thermal loads effects on Nd:YAG solar-lasers performance, research details will be given afterward. Some literatures<sup>1–3,6,7,9,21–29</sup> were made for the solar-laser efficiency improvement, whereas others included laser beam quality enhancements.<sup>11,26–28,30–35</sup>

Research details will be given for both multimode and monomode (fundamental-mode) solar-laser operations, respectively.

#### 3.1 Main Research in Multimode Solar-Laser Operation

To clearly expose all the previous multimode solar-laser research studies, details (data and results) are summarized in the following Figs. 5–20.

##### 3.1.1 Discussions

Collection efficiency is generally regarded as a primary figure of merit for solar-laser systems. The second is the beam quality factors ( $M_x^2$  and  $M_y^2$ ), which is defined by the ratio between laser beam divergence and divergence of diffraction-limited Gaussian beam.<sup>31</sup>

One of the main problems preventing wide spreading of solar-pumped lasers is the relatively low efficiency, compared with diode-pumped lasers. Since the first report of “A sun-pumped c w one-watt laser” in 1966,<sup>1</sup> optical and laser material advances have continued to improve solar-laser performance. Several pumping architectures have been proposed for solar-pumped solid-state lasers with the intention of achieving the maximum transfer and absorption efficiencies from the pump source to the laser crystal.<sup>8</sup> These laser systems can have either side-pumping or end-pumping configurations. The most efficient laser systems have end-pumping approaches because of the high absorption efficiency of the pump light by the laser crystal. In turn the

Sources	Young C. G., 1966	Solar-laser head configuration
Primary stage concentrator	Modified Cassegrain sun-tracking telescope 61 cm diameter, 0.29 m <sup>2</sup> effective collection area	
Secondary stage concentrator	x	
Pump-cavity	Conical-pump-cavity	
Active medium	Nd:YAG rod	
Pumping configuration	End-side-pumping	
Multi-mode laser power (W)	1 (c w: continuous wave)	
Multi-mode collection efficiency, (W/m <sup>2</sup> )	3.45	
Brightness figure of merit (W)	x	
M <sup>2</sup>	x	

Fig. 5 Young C. G., (1966).<sup>1</sup>

Sources	Arashi H. et al., 1984	Solar-laser head configuration
Primary stage concentrator	78.5 m <sup>2</sup> , effective collection area, parabolic mirror	
Secondary stage concentrator	Mounting directly at the focus	
Pump-cavity	Tube	
Active medium	4 mm diameter, 75 mm length Nd:YAG rod	
Pumping configuration	Quasi side-pumping	
Multi-mode laser power (W)	18 (c w)	
Multi-mode collection efficiency, (W/m <sup>2</sup> )	0.23	
Brightness figure of merit (W)	x	
M <sup>2</sup>	x	

Fig. 6 Arashi H. et al., (1984).<sup>2</sup>

Sources	Weksler M. and Shwartz J., 1988	Solar-laser head configuration
Primary stage concentrator	Segmented primary concentrator: 600 spherical mirrors, 38.5 m <sup>2</sup> , effective collection area	
Secondary stage concentrator	2D - CPC	
Pump-cavity	2D - CPC	
Active medium	Nd:YAG rod	
Pumping configuration	Side-pumping	
Multi-mode laser power (W)	60 (c w)	
Multi-mode collection efficiency, (W/m <sup>2</sup> )	1.56	
Brightness figure of merit (W)	x	
M <sup>2</sup>	x	

Fig. 7 Weksler M. and Shwartz J., (1988).<sup>3</sup>

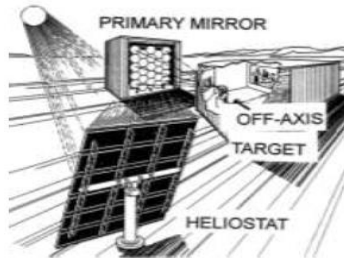
Sources	Jenkins D. G., 1996	Solar-laser head configuration
Primary stage concentrator	12.12 m <sup>2</sup> , effective collection area, 25 hexagonal segments, parabolic mirror	
Secondary stage concentrator	tailored non-imaging secondary concentrator	
Pump-cavity	x	
Active medium	10 mm diameter Nd:YAG rod	
Pumping configuration	Side-pumping	
Multi-mode laser power (W)	57	
Multi-mode collection efficiency, (W/m <sup>2</sup> )	4.7	
Brightness figure of merit (W)	x	
M <sup>2</sup>	x	

Fig. 8 Jenkins D. G., (1996).<sup>21</sup>

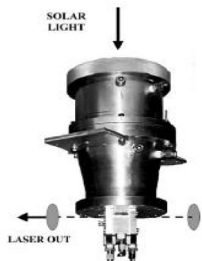
Sources	Lando M. et al., 2003	Solar-laser head configuration
Primary stage concentrator	6.75 m <sup>2</sup> , effective collection area, segmented parabolic mirror	
Secondary stage concentrator	3D - CPC	
Pump-cavity	2D - CPC cavity	
Active medium	10 mm diameter, 130 mm length Nd:YAG rod	
Pumping configuration	Side-pumping	
Multi-mode laser power (W)	46 (c w)	
Multi-mode collection efficiency, (W/m <sup>2</sup> )	6.7	
Brightness figure of merit (W)	0.00033	
M <sup>2</sup>	M <sup>2</sup> <sub>x</sub> = 7, M <sup>2</sup> <sub>y</sub> = 76 Multi-mode laser power 17 W, Brightness figure of merit 0.032 W	

Fig. 9 Lando M. et al., (2003).<sup>9</sup>

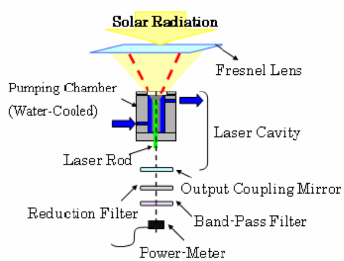
Sources	Yabe Y. et al., 2007	Solar-laser head configuration
Primary stage concentrator	1.3 m <sup>2</sup> , effective collection area, Fresnel lens	
Secondary stage concentrator	x	
Pump-cavity	Pumping chamber	
Active medium	9 mm diameter, 100 mm length Cr: Nd:YAG rod	
Pumping configuration	End-pumping	
Multi-mode laser power (W)	24.4 (c w)	
Multi-mode collection efficiency, (W/m <sup>2</sup> )	18.7	
Brightness figure of merit (W)	x	
M <sup>2</sup>	x	

Fig. 10 Yabe Y. et al., (2007).<sup>6</sup>

Sources	Liang D. and Almeida J., 2011	Solar-laser head configuration
Primary stage concentrator	0.64 m <sup>2</sup> , effective collection area, Fresnel lens	
Secondary stage concentrator	DTIRC	
Pump-cavity	Conical-pump-cavity	
Active medium	4 mm diameter, 34 mm length Nd:YAG rod	
Pumping configuration	End-side-pumping	
Multi-mode laser power (W)	12.3 (c w)	
Multi-mode collection efficiency, (W/m <sup>2</sup> )	19.3	
Brightness figure of merit (W)	0.014	
M <sup>2</sup>	M <sup>2</sup> = 10.6, Multi-mode laser power 9.7W, Brightness figure of merit 0.086 W	

Fig. 11 Liang D. and Almeida J., (2011).<sup>22</sup>

Sources	Dinh T. H. et al., 2012	Solar-laser head configuration
Primary stage concentrator	4 m <sup>2</sup> , effective collection area, Fresnel lens	
Secondary stage concentrator	x	
Pump-cavity	Conical-pump-cavity	
Active medium	6 mm diameter, 100 mm length Nd:YAG rod	
Pumping configuration	End-side-pumping	
Multi-mode laser power (W)	120 (c w)	
Multi-mode collection efficiency, (W/m <sup>2</sup> )	30	
Brightness figure of merit (W)	0.0066	
M <sup>2</sup>	137	

Fig. 12 Dinh T. H. et al., (2012).<sup>23</sup>

Sources	Almeida J. et al., 2012	Solar-laser head configuration
Primary stage concentrator	2.88 m <sup>2</sup> , effective collection area, parabolic mirror	
Secondary stage concentrator	Light guide	
Pump-cavity	2D – CPC-cavity	
Active medium	4 mm diameter, 30 mm length Nd:YAG rod	
Pumping configuration	Side-pumping	
Multi-mode laser power (W)	27.7 (c w)	
Multi-mode collection efficiency, (W/m <sup>2</sup> )	9.6	
Brightness figure of merit, (W)	0.16	
M <sup>2</sup>	M <sup>2</sup> <sub>x</sub> = 8.9, M <sup>2</sup> <sub>y</sub> = 9.6 Multi-mode laser power 24.7W, Brightness figure of merit 0.29 W	

Fig. 13 Almeida J. et al., (2012).<sup>30</sup>



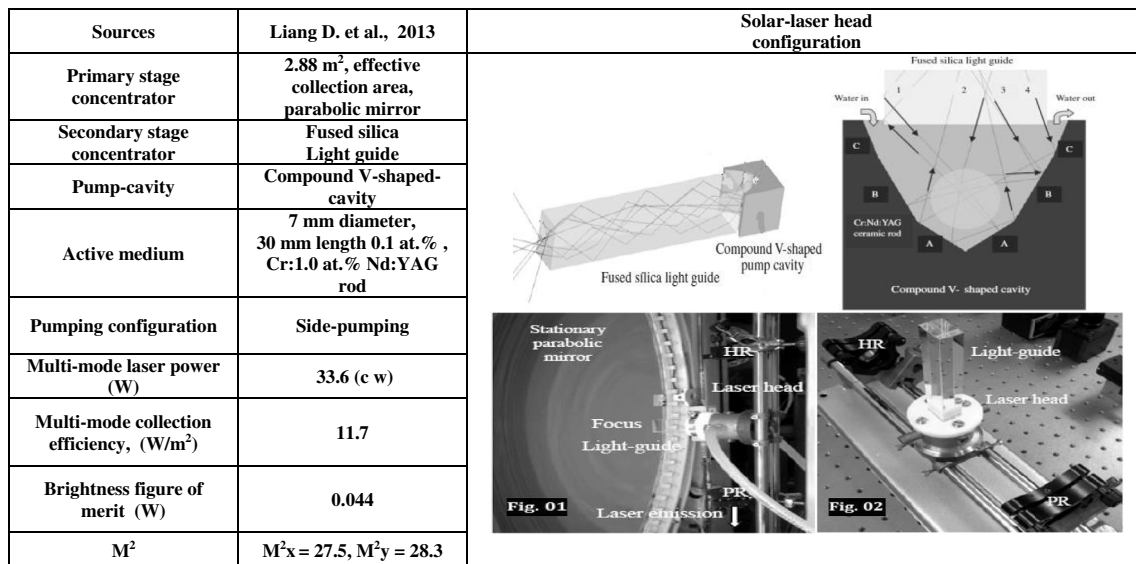


Fig. 14 Liang D. et al., (2013).<sup>7</sup>

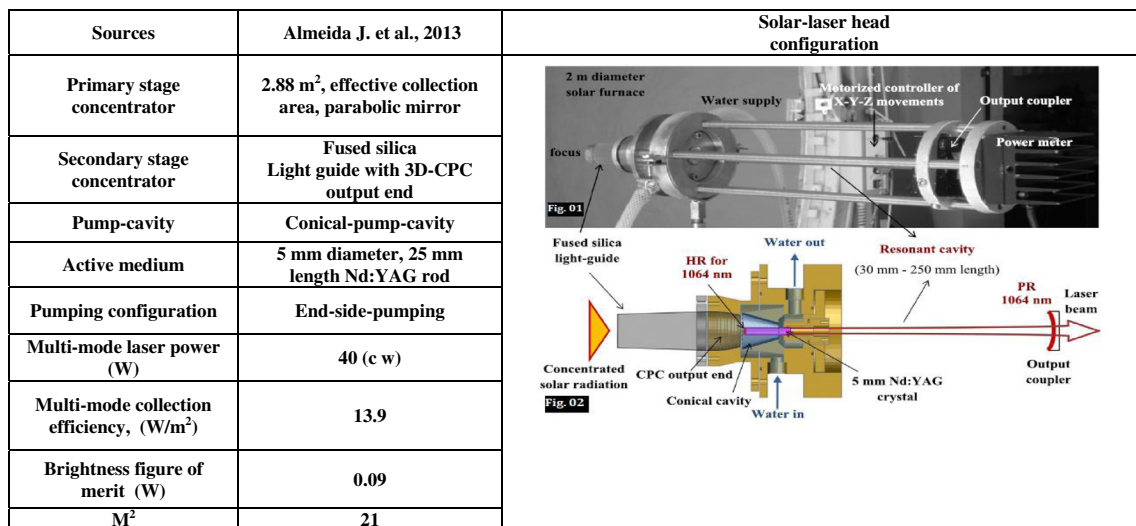


Fig. 15 Almeida J. et al., (2013).<sup>24</sup>

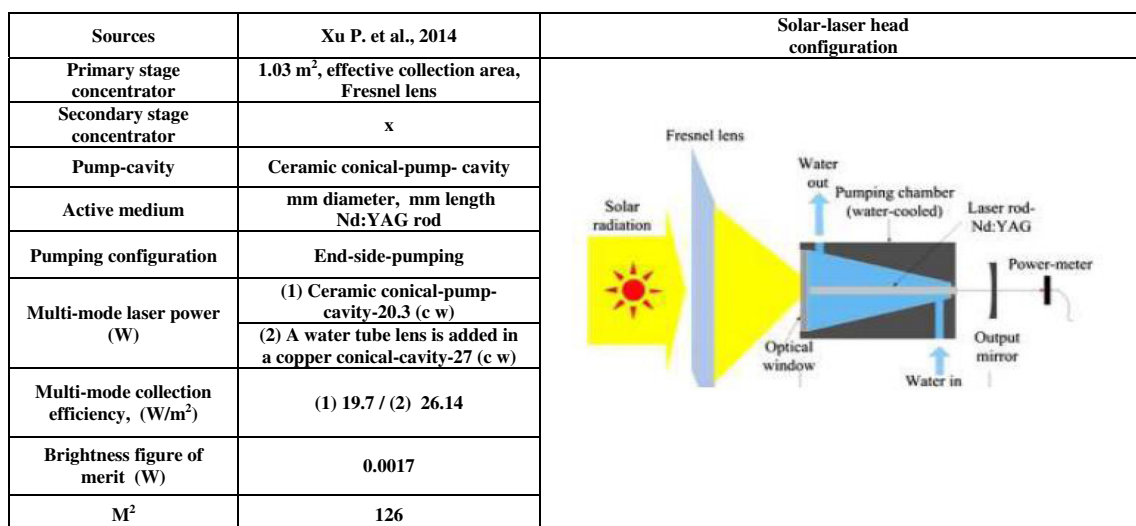


Fig. 16 Xu P. et al., (2014).<sup>25</sup>

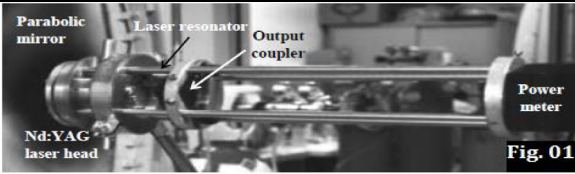
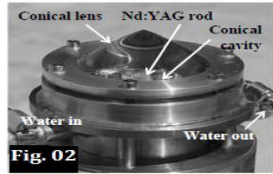
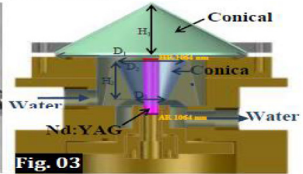
Sources	Almeida J. et al., 2015	Solar-laser head configuration
Primary stage concentrator	2.65 m <sup>2</sup> , effective collection area, parabolic mirror	  
Secondary stage concentrator	Fused silica conical lens	
Pump-cavity	Conical-pump-cavity	
Active medium	5 mm diameter, 25 mm length, 1.0 at.% Nd:YAG rod	
Pumping configuration	End-side-pumping	
Multi-mode laser power (W)	56 (c w)	
Multi-mode collection efficiency, (W/m <sup>2</sup> )	21.1	
Brightness figure of merit (W)	0.028	
M <sup>2</sup>	44.7	

Fig. 17 Almeida J. et al., (2015).<sup>26</sup>

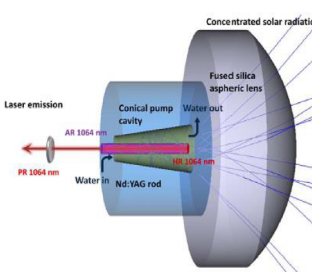
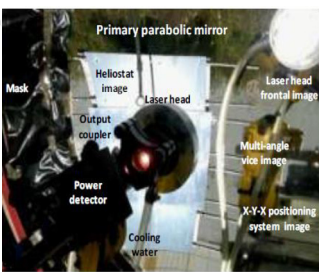
Sources	Liang D. et al., 2016	Solar-laser head configuration
Primary stage concentrator	1.28 m diameter, (1.17 m <sup>2</sup> effective collection area), parabolic mirror	 
Secondary stage concentrator	Fused silica aspheric lens	
Pump-cavity	Conical-pump-cavity	
Active medium	4 mm diameter, 35 mm length, Nd:YAG rod	
Pumping configuration	End-side-pumping	
Multi-mode laser power (W)	29.3 (c w)	
Multi-mode collection efficiency, (W/m <sup>2</sup> )	25	
Brightness figure of merit (W)	0.01	
M <sup>2</sup>	54.13	

Fig. 18 Liang D. et al., (2016).<sup>27</sup>

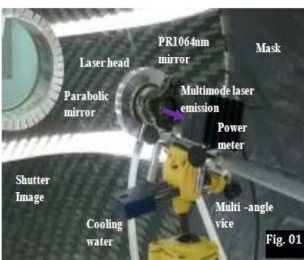
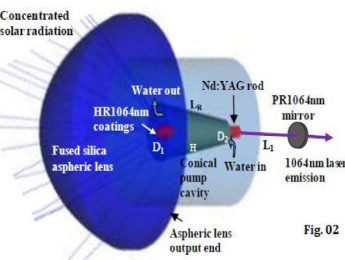
Sources	Liang D. et al., 2017	Solar-laser head configuration
Primary stage concentrator	1.4 m diameter, parabolic mirror	 
Secondary stage concentrator	Fused silica aspheric lens	
Pump-cavity	Conical-pump-cavity	
Active medium	4 mm diameter, 35 mm length, Nd:YAG rod	
Pumping configuration	End-side-pumping	
Multi-mode laser power (W)	37.2 (c w)	
Multi-mode collection efficiency, (W/m <sup>2</sup> )	31.5	
Brightness figure of merit (W)	0.013	
M <sup>2</sup>	53.5	

Fig. 19 Liang D. et al., (2017).<sup>28</sup>

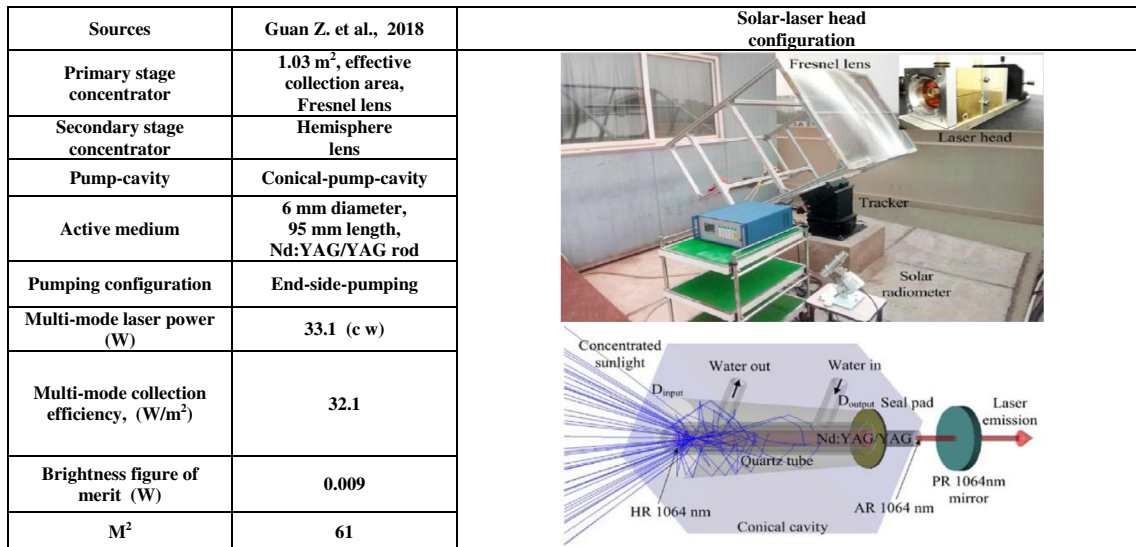


Fig. 20 Guan Z. et al., (2018).<sup>29</sup>

thermal loading effects caused by nonuniform distribution of pump-light in these pumping configurations negatively affect the laser beam quality. To prove that, research results will be discussed below.

In multimode regime, by using the end-pumping method, high collection efficiency of 30.0 W/m<sup>2</sup> was attained by pumping a large Nd:YAG rod through a large Fresnel lens.<sup>23</sup> However, very large  $M_x^2 = M_y^2 = 137$  factors have been associated with this approach, resulting in very poor beam quality. Since the report of this result, many research studies have been made to improve both, the collection efficiency and the beam quality factors of the solar-laser systems.

About 31.5 W/m<sup>2</sup> collection efficiency was achieved by pumping a 4-mm diameter, 35-mm length Nd:YAG rod through 1.18 m<sup>2</sup> area parabolic mirror.<sup>28</sup> Although, it was only slightly higher than the previous record value obtained by Ref. 23, this research gave rise to significant improvement of the beam quality factors with  $M^2 = 53.5$ . This value is still large to obtain a high-laser beam quality. Record-high collection efficiency of 32.1 W/m<sup>2</sup> was attained by pumping a large

Nd:YAG rod through a large Fresnel lens.<sup>29</sup> Despite the high collection efficiency, the  $M^2$  factors were large ( $M_x^2 = M_y^2 = 61$ ), being 1.14 times higher than the previous result.

Side-pumping configuration presents high beam quality as it allows uniform absorption distribution along the rod axis and spreads the absorbed power within this laser medium, reducing the associated thermal loading problems. In contrast, this pumping method leads to low collection efficiency because of its low absorption efficiency.

A multi-mode collection efficiency of 9.6 W/m<sup>2</sup> with the lowest  $M^2$  factors ( $M_x^2 = 8.9$  and  $M_y^2 = 9.6$ ) was obtained by Ref. 30 by pumping a large Nd:YAG rod through a parabolic mirror.

### 3.2 Main Research in TEM<sub>00</sub>-Mode Solar-Laser Operation

To complete the exposition of previous solar-laser research, details (data and results) of the TEM<sub>00</sub>-mode solar-laser research are summarized in the following Figs. 21–28.

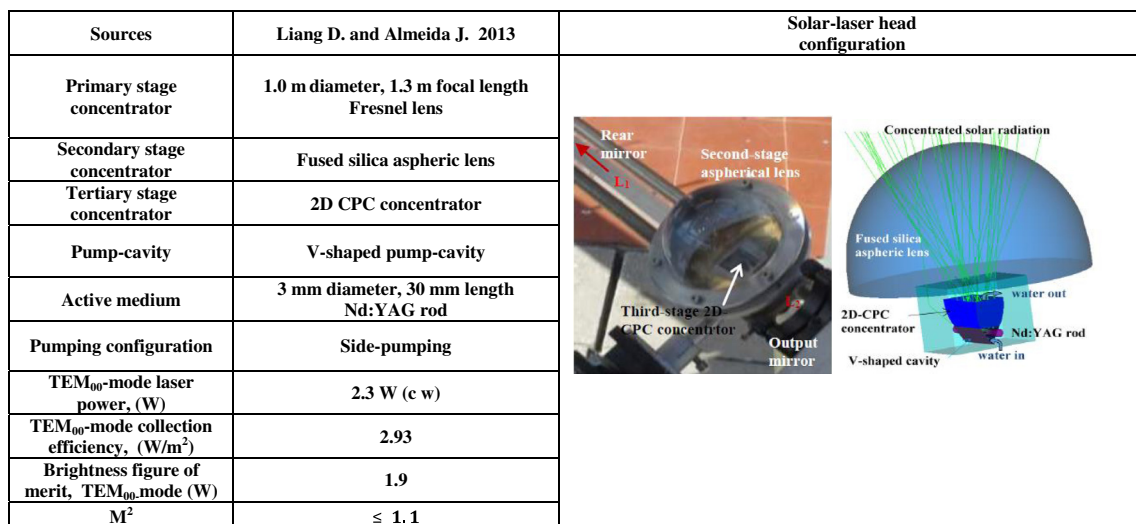


Fig. 21 Liang D. and Almeida J., (2013).<sup>36</sup>

Sources	Liang D. et al., 2015	Solar-laser head configuration
Primary stage concentrator	2m diameter, (2.3 m <sup>2</sup> effective collection area), parabolic mirror	
Secondary stage concentrator	Fused silica light guide	
Tertiary stage concentrator	2D CPC concentrator	
Pump-cavity	V-shaped pump-cavity	
Active medium	3 mm diameter, 30 mm length Nd:YAG rod	
Pumping configuration	Side-pumping	
TEM <sub>00</sub> -mode laser power, (W)	4.4 W (c w)	
TEM <sub>00</sub> -mode collection efficiency, (W/m <sup>2</sup> )	1.9	
Brightness figure of merit, TEM <sub>00</sub> -mode (W)	4.0	
M <sup>2</sup>	≤ 1.05	

Fig. 22 Liang D. et al., (2015).<sup>32</sup>

Sources	Almeida J. et al., 2015	Solar-laser head configuration
Primary stage concentrator	2m diameter, (1.92 m <sup>2</sup> effective collection area), parabolic mirror	
Secondary stage concentrator	Fused silica light guide	
Tertiary stage concentrator	2D-trapezoidal output section of Light guide	
Pump-cavity	2V-shaped pump-cavity	
Active medium	4 mm diameter, 30 mm length Nd:YAG rod	
Pumping configuration	Side-pumping	
TEM <sub>00</sub> -mode laser power, (W)	5.5 W (c w)	
TEM <sub>00</sub> -mode collection efficiency, (W/m <sup>2</sup> )	2.84	
Brightness figure of merit, TEM <sub>00</sub> -mode (W)	3.52	
M <sup>2</sup>	≤ 1.25	

Fig. 23 Almeida J. et al., (2015).<sup>37</sup>

Sources	Vistas C. R. et al., 2015	Solar-laser head configuration
Primary stage concentrator	1.5 m diameter, (1.1 m <sup>2</sup> effective collection area), parabolic mirror	
Secondary stage concentrator	Fused silica semi-cylindrical lens	
Tertiary stage concentrator	x	
Pump-cavity	2V-shaped pump-cavity	
Active medium	3.5 mm diameter, 34 mm length Nd:YAG rod	
Pumping configuration	Side-pumping	
TEM <sub>00</sub> -mode laser power, (W)	4.0 W (c w)	
TEM <sub>00</sub> -mode collection efficiency, (W/m <sup>2</sup> )	3.6	
Brightness figure of merit, TEM <sub>00</sub> -mode (W)	3.0	
M <sup>2</sup>	M <sup>2</sup> <sub>x</sub> ≤ 1.2, M <sup>2</sup> <sub>y</sub> ≤ 1.1	

Fig. 24 Vistas C. R. et al., (2015).<sup>34</sup>

Sources	Liang D. et al., 2016	Solar-laser head configuration
Primary stage concentrator	1.33m diameter, (1.13 m <sup>2</sup> effective collection area), parabolic mirror	
Secondary stage concentrator	Ellipsoid-shaped fused silica concentrator	
Tertiary stage concentrator	x	
Pump-cavity	2V-shaped pump-cavity	
Active medium	4 mm diameter, 25 mm length Nd:YAG rod	
Pumping configuration	Side-pumping	
TEM <sub>00</sub> -mode laser power, (W)	4.5 W (c w)	
TEM <sub>00</sub> -mode collection efficiency, (W/m <sup>2</sup> )	4.0	
Brightness figure of merit, TEM <sub>00</sub> -mode (W)	3.72	
M <sup>2</sup>	≤ 1.1	

Fig. 25 Liang D. et al., (2016).<sup>27</sup>

Sources	Liang D. et al., 2017	Solar-laser head configuration
Primary stage concentrator	2m diameter, (1.18 m <sup>2</sup> effective collection area), parabolic mirror	
Secondary stage concentrator	Fused silica aspheric lens	
Tertiary stage concentrator	x	
Pump-cavity	V-shaped pump-cavity	
Active medium	4 mm diameter, 35 mm length Nd:YAG rod	
Pumping configuration	End-side-pumping	
TEM <sub>00</sub> -mode laser power, (W)	9.3 W (c w)	
TEM <sub>00</sub> -mode collection efficiency, (W/m <sup>2</sup> )	7.9	
Brightness figure of merit, TEM <sub>00</sub> -mode (W)	6.46	
M <sup>2</sup>	≤ 1.2	

Fig. 26 Liang D. et al., (2017).<sup>28</sup>

### 3.2.1 Discussions

The same conclusions remain valid for TEM<sub>00</sub>-mode operation. The end-pumping configuration provides high collection efficiency. However, high M<sup>2</sup> factors have been associated with this approach. Record-high collection efficiency of 7.9 W/m<sup>2</sup> was reported by Ref. 28 with only 1.2 as M<sup>2</sup> factors. In contrast, the side-pumping configuration leads to low collection efficiency with very low M<sup>2</sup> factors. Record-low M<sup>2</sup> factors <1.05 have been reported by Refs. 11, 32, and 35. Low collection efficiency was registered for all these literatures.

### 4 TEM<sub>00</sub>-Mode Solar Laser Power Stability

In this last part of this paper, we give a description of the output power measurement process of a solar-laser system

using side-pumping and end-pumping methods, respectively, to show that in addition to the high solar-laser beam quality, the side-pumping configuration presents the advantage to be able to produce a stable TEM<sub>00</sub>-mode solar-laser power.

Using the side-pumping method, low TEM<sub>00</sub>-mode solar-laser power was measured during 240 s, with the maximum output power variation being <1.7%. The Gaussian fundamental-mode profile was also found stable during the measurement.<sup>11</sup> In the same experimental conditions as the previous pumping-method, the end-pumped laser,<sup>28</sup> provided high TEM<sub>00</sub>-mode laser output power. Strong oscillations of 12% were observed during the measurement process of 240 s. These oscillations are due to high thermal lensing effect and consequently short thermal focal lens, which make the TEM<sub>00</sub>-mode laser output power very sensible to both pumping flux and temperature variation of the laser rod.

Sources	Bouadjemine R. et al., 2017	Solar-laser head configuration
Primary stage concentrator	2 m diameter, (1.18 m <sup>2</sup> effective collection area), parabolic mirror	
Secondary stage concentrator	Fused silica twisted light guide	
Tertiary stage concentrator	2D CPC concentrator	
Pump-cavity	2V-shaped pump-cavity	
Active medium	3 mm diameter, 50 mm length Nd:YAG rod	
Pumping configuration	Side-pumping	
TEM <sub>00</sub> -mode laser power, (W)	2.3 W (c w)	
TEM <sub>00</sub> -mode collection efficiency, (W/m <sup>2</sup> )	1.96	
Brightness figure of merit, TEM <sub>00</sub> -mode (W)	2.2	
M <sup>2</sup>	≤ 1.05	

Fig. 27 Bouadjemine R. et al., (2017).<sup>35</sup>

Sources	Mehellou S. et al., 2017	Solar-laser head configuration
Primary stage concentrator	2 m diameter, (1.18 m <sup>2</sup> effective collection area), parabolic mirror	
Secondary stage concentrator	Fused silica twisted light guide	
Tertiary stage concentrator	2D CPC concentrator	
Pump-cavity	2V-shaped pump-cavity	
Active medium	3 mm diameter, 50 mm length Nd:YAG rod	
Pumping configuration	Side-pumping	
TEM <sub>00</sub> -mode laser power, (W)	2.7 W (c w)	
TEM <sub>00</sub> -mode collection efficiency, (W/m <sup>2</sup> )	2.3	
Brightness figure of merit, TEM <sub>00</sub> -mode (W)	2.45	
M <sup>2</sup>	≤ 1.05	

Fig. 28 Mehellou S. et al., (2017).<sup>11</sup>

The end-pumped laser offered the maximum TEM<sub>00</sub>-mode solar-laser collection efficiency, but also suffered from a very strong thermal load effect, much more than the 1.7% of the side-pumped laser. Figure 29 shows a favorable result in fundamental mode laser beam stability of <12% for the end-pumped laser.

During the measurement process, however, it was found not easy to maintain a perfect Gaussian mode profile due to the strong thermal load effect of this type of laser. Solar irradiance variation of <0.5%, cooling water temperature oscillation of <2 deg during the measurement were found sufficient to change a solar laser beam with Gaussian profile into a low-order mode beam with a two-mode, sometimes a four-mode or even a doughnut-shaped profiles were observed.<sup>11</sup>

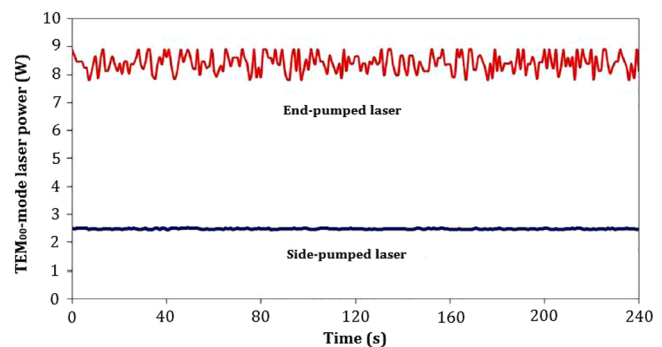


Fig. 29 Time dependent TEM<sub>00</sub>-mode solar-laser power variations of both end-pumped laser<sup>28</sup> and side-pumped laser.<sup>11</sup>

## 5 Conclusion

The growing importance of solar-pumped lasers has attracted considerable attention. Many studies have already been carried out to improve solar-laser efficiencies. As the sunlight does not provide enough flux to initiate laser emission, additional focusing optics are needed to both collect and concentrate the solar radiation to excite laser medium. Parabolic mirrors have long been explored to achieve tight focusing of incoming solar radiation. Significant progresses in solar laser efficiency have been made with the adoption of Fresnel lenses as primary solar concentrators.

To maximize the solar radiation that impinges on the laser crystal, the 2-D-CPC, the 3-D-CPC and the V-shaped pump cavity are usually used as secondary and tertiary concentrators in solar-lasers because they can either compress or wrap the concentrated solar radiations from their input aperture to the laser rod and give an additional concentration.

Moreover, to improve solar laser performance, several pumping architectures have been proposed. These pumping architectures can be either side-pumping or end-pumping configurations.

The most efficient laser systems have end-pumping configurations, the thermal loading effects caused by nonuniform distribution of absorbed pump light typical in these pumping configurations affect negatively their laser beams quality, high collection efficiency can be achieved with these pumping approaches. Record-high multimode collection efficiency of 32.1 and 7.9 W/m<sup>2</sup> for TEM<sub>00</sub>-mode regime were attained.

In the side-pumping configuration there are a lot of heat around the solar laser rod (quite different from that of LD-pumped) so the uniform distribution of pumping flux along the rod is important for solar-lasers due to the heat removal issue. Therefore, the side-pumping is an effective configuration for producing high laser beam quality as it allows a uniform absorption distribution along the rod axis, reducing the associated thermal loading problems.

It gives the lowest  $M^2$  beam quality factors, <10 for multimode and <1.05 for TEM<sub>00</sub>-mode operating regimes. This pumping method also makes it possible to obtain a stable TEM<sub>00</sub>-mode solar-pumped laser output power.

Finally, it was worth noting that by pumping smaller diameter rods it can lead to meliorate the solar-laser beam quality of high efficiency solar-pumping schemes. Furthermore the thermal management of end-pumped lasers can be greatly improved by the use of composite rods. Laser crystals have become available with sections of undoped host material on one or both ends. These end caps are diffusion bonded to the doped laser crystal. Composite rods are proven to provide a very effective way to reduce temperature and stresses at the face of end-pumped lasers. Regarding the collection efficiency of side-pumped lasers, it can be significantly enhanced by the use of the power scaling method.

## References

- C. G. Young, "A sun-pumped c. w. one-watt," *Laser Appl. Opt.* **5**(6), 993–995 (1966).
- H. Arashi et al., "Solar-pumped c. w. 18 W Nd:YAG laser," *Jpn. J. Appl. Phys.* **23**(8), 1051–1053 (1984).
- M. Weksler and J. Schwartz, "Solar-pumped solid-state lasers," *IEEE J. Quantum Electron.* **24**(6), 1222–1228 (1988).
- D. Cooke, "Sun-pumped lasers: revisiting an old problem with non-imaging optics," *Appl. Opt.* **36**, 7541–7546 (1992).
- R. M. J. Benmair et al., "Solar-pumped Er, Tm, Ho:YAG laser," *Opt. Lett.* **15**(1), 36–33 (1990).
- Y. Yabe et al., "High efficiency and economical solar energy pumped laser with Fresnel lens and chromium co-doped laser medium," *Appl. Phys. Lett.* **90**(26), 261120 (2007).
- D. Liang, J. Almeida, and E. Guillot, "Side-pumped continuous-wave Cr:Nd:YAG ceramic solar laser," *Appl. Phys. B* **111**(2), 305–311 (2013).
- J. P. Geraldès and D. Liang, "An alternative solar pumping approach by a light guide assembly elliptical-cylindrical cavity," *Solar Energy Mater. Solar Cells* **92**(8), 836–843 (2008).
- M. Lando et al., "A solar-pumped Nd:YAG laser in the high collection efficiency regime," *Opt. Commun.* **222**(1–6), 371–381 (2003).
- M. Lando et al., "High-brightness-solar-pumped Nd:YAG laser design," *Proc. SPIE* **2426**, 478–490 (1995).
- S. Mehellou et al., "Stable solar-pumped TEM<sub>00</sub>-mode 1064 nm laser emission by a monolithic fused silica twisted light guide," *Solar Energy* **155**, 1059–1071 (2017).
- C. Pfister et al., "Thermal beam distortions in end-pumped Nd:YAG, Nd:GSGG and Nd:YLF rods," *IEEE J. Quantum Electron.* **30**(7), 1605–1615 (1994).
- R. Weber et al., "Cooling schemes for longitudinally diode laser-pumped Nd:YAG rods," *IEEE J. Quantum Electron.* **34**(6), 1046–1053 (1998).
- E. Safari and A. Kachanov, "Estimation of thermal lensing effect in the high-power end-pumped direct-cut crystal lasers," *Opt. Laser Technol.* **38**(7), 534–539 (2006).
- W. Koehner, *Solid-State Laser Engineering*, 6th ed., Springer series in optical sciences, pp. 245–278, Springer, London (2006).
- W. Koehner, "Thermal lensing in a Nd:YAG laser rod," *Appl. Opt.* **9**(11), 2548 (1970).
- S. Chénais et al., "On thermal effects in solid-state lasers: the case of ytterbium doped materials," *Progr. Quantum Electron.* **30**(4), 89–153 (2006).
- M. Sovizi and R. Massudi, "Thermal distribution calculation in diode pumped Nd:YAG laser rod by boundary element method," *Opt. Laser Technol.* **39**(1), 46–52 (2007).
- Y. S. Huang, H. L. Tsai, and F. L. Chang, "Thermo-optic effects affecting the high pump power end pumped solid state lasers: modeling and analysis," *Opt. Commun.* **273**(2), 515–525 (2007).
- S. D. Moustafa, "Finite element analysis of thermal effects in diode end-pumped solid-state lasers," *Adv. Opt. Techn.* **9256053**, 15 (2017).
- D. Jenkins et al., "A solar-pumped Nd:YAG laser with a record efficiency of 4.7 watt/m<sup>2</sup>," *Bull. Israel Phys. Soc.* **101** (1996).
- D. Liang and J. Almeida, "Highly efficient solar-pumped Nd:YAG laser," *Opt. Express* **19**(27), 26399 (2011).
- T. H. Dinh et al., "120 Watt c. w. solar-pumped laser with a liquid light-guide lens and an Nd:YAG rod," *Opt. Lett.* **37**(13), 2670–2673 (2012).
- J. Almeida et al., "A 40 W c. w. Nd:YAG solar laser pumped through a heliostat: a parabolic mirror system," *Laser Phys.* **23**(6), 065801 (2013).
- P. Xu et al., "High-efficiency solar-pumped laser with a grooved Nd:YAG rod," *Appl. Opt.* **53**(18), 3941–3944 (2014).
- J. Almeida et al., "Highly efficient end-side-pumped Nd:YAG solar laser by a heliostat-parabolic mirror system," *Appl. Opt.* **54**(8), 1970–1978 (2015).
- D. Liang, J. Almeida, and C. R. Vistas, "25 W/m<sup>2</sup> collection efficiency solar-pumped Nd:YAG laser by a heliostat-parabolic mirror system," *Appl. Opt.* **55**(27), 7712–7716 (2016).
- D. Liang et al., "Solar-pumped Nd:YAG laser with 31.5 W/m<sup>2</sup> multimode and 7.9 W/m<sup>2</sup> TEM<sub>00</sub>-mode collection efficiencies," *Sol. Energy Mater. Sol. Cells* **159**, 435–439 (2017).
- Z. Guan et al., "32.1 W/m<sup>2</sup> c. w. solar-pumped laser with a bonding Nd:YAG/YAG rod and a Fresnel lens," *Opt. Laser Technol.* **107**, 158–161 (2018).
- J. Almeida, D. Liang, and E. Guillot, "Improvement in solar-pumped Nd:YAG laser beam brightness," *Opt. Laser Technol.* **44**(7), 2115–2119 (2012).
- D. Liang and J. Almeida, "Solar-pumped TEM<sub>00</sub>-mode Nd:YAG laser," *Opt. Express* **21**(21), 25107 (2013).
- D. Liang et al., "Solar-pumped TEM<sub>00</sub>-mode Nd:YAG laser by a heliostat-parabolic mirror system," *Sol. Energy Mater. Sol. Cells* **134**, 305–308 (2015).
- D. Liang et al., "High-efficiency solar pumped TEM<sub>00</sub>-mode Nd:YAG laser," *Sol. Energy Mater. Sol. Cells* **145**, 397–402 (2016).
- C. V. Vistas, D. Liang, and J. Almeida, "Solar-pumped TEM<sub>00</sub>-mode laser simple design with a grooved Nd:YAG rod," *Solar Energy* **122**, 1325–1333 (2015).
- R. Bouadjemine et al., "Stable TEM<sub>00</sub>-mode Nd:YAG solar laser operation by a twisted fused silica light-guide," *Opt. Laser Technol.* **97**, 1–11 (2017).
- D. Liang and J. Almeida, "Solar-pumped TEM<sub>00</sub>-mode Nd:YAG laser," *Opt. Express* **21**(21), 25107 (2013).
- J. Almeida et al., "E. 5.5W c. w. TEM<sub>00</sub>-mode Nd:YAG solar laser by a light guide/2V pump cavity," *Appl. Phys. B* **121**(4), 473–482 (2015).

**Mehellou Saïd** is a doctor in physics, solar laser. He is a member of the Laboratory of Exploitation and Valorization of Saharian Energy Resources (LEVRES) and a teacher at the Eloued University, Algeria.

**Rehouma Ferhat** is a professor in physics, optoelectronics. He is a director of the Laboratory of Exploitation and Valorization of Saharian Energy Resources (LEVRES) and a professor at the Eloued University, Algeria.

**Hamrouni Nouredine** is a member of the Laboratory of Exploitation and Valorization of Saharian Energy Resources (LEVRES). He is a PhD student in solar lasers.

**Bouras Leila** is a member at the Laboratory of Exploitation and Valorization of Saharian Energy Resources (LEVRES). She is a PhD student in solar lasers.